An Experimental Study to Apply an Absorption Refrigeration Cycle as a Dehumidifier in Humidification-Dehumidification Solar Desalination System

S. Aghajani Afghan[1], R. Shafaghat*[1], A. Aghajani Afghan[1], S. M. Hosseinalipour[2]

[1] *Sea-based Energy Research Group, Mechanical Engineering Department, Babol Noshirvani University of Technology, Babol, Iran*
[2] *Department of Mechanical Engineering, Science and Technology University, Tehran, Iran*

PAPER INFO

ABSTRACT

In this paper, the performance of a hybrid humidification-dehumidification (HDH) desalination system is experimentally studied. The system operates as an Open-Air Closed-Water cycle and utilizes a solar air heater to heat the input air to the humidifier. An Ammonia absorption refrigeration cooling cycle is used to condense the humid air, producing fresh water. Parameters such as temperature and relative humidity were measured in different stages of the system by using humidity and temperature sensors, and the thermodynamic analysis was carried out using EES software. The effects of the mass flow rate and temperature of the inlet air flow on the rate of desalination, COP, GOR, and the efficiency of the humidifier and the dehumidifier were studied. The analysis proved that the highest rate of water production and GOR were 150 g/h and 1.2, respectively. It was also perceived that with an increase in the air mass flow rate, the rate of water production and COP increased, while GOR and the efficiency of the dehumidifier diminished. This is while the efficiency of the humidifier remains nearly constant. It was also concluded that an increase in the temperature of the input air, leads to a fall in the GOR, while the other parameters show an increasing trend. Following the economic analysis of the system, the CPL was found to be $0.16 /L.

doi: 10.5829/ijee.2023.14.04.06

INTRODUCTION

One of the most important mankind concerns throughout history has been the supply of fresh water. All human civilizations were found near large rivers. Today, with an increase in world population, demands for fresh water are also increasing. It is predicted that by the year 2030, fresh water sources will be 40% less than the demand [1]. This has encouraged many researchers to develop desalination systems. In addition to that, researchers are seeking technologies that work with low-temperature, renewable energy sources; rather than those that require high-temperature energy sources [2]. This can ultimately contribute to solving water scarcity and energy shortage. One of these systems is the HDH desalination setup which has notable advantages, such as small size, simple design, low maintenance cost, and ability to start with wasted heat or renewable energy sources [3].

It is noteworthy that most of the HDH desalination setups are operated by solar energy [4]. Many researchers have studied the relationship between the rate of fresh water output and the intensity of solar radiation in HDH systems. In a study conducted by Orfi et al. [5], it was concluded that the water output is directly proportional to radiation intensity. Soomro et al. [6] showed that higher water output and GOR in their proposed HDH system belonged to the months in which the radiation intensity was greater. Considering the crucial importance of sunlight in the operation of HDH systems, there have been multiple kinds of research regarding the operation of HDH systems in unsuitable climates. Cichoń and Worek [7] studied the operation of an HDH system under an unsuitable climate condition and decreased dehumidification temperature. Their study focused on producing water with better GOR in cold climate conditions with low radiation intensity.

---

*Corresponding Author Email: *rshafaghat@nit.ac.ir* (R. Shafaghat)

Considering the fact that HDH cycles require high-temperature energy sources to increase the temperature of air or saline water and low-temperature sources for dehumidification of humid air, many researchers have attempted to propose hybrid systems consisting of HDH systems as well as refrigeration cycles [8]. Lawal et al. [9] studied an HDH-REF cycle theoretically. In the studied case, the input seawater was cooled in a Vapor-Compression Refrigeration (VCR) system before the dehumidification process to increase the rate of dehumidification. In addition, the heat load of the VCR condenser was used to heat the water/air entering the humidification process. The results indicated that the heated air cycle was more efficient in terms of energy and exergy generation in comparison to the heated water cycle [10]. They studied and optimized a CAOW HDH system coupled with an Ammonia-Water VAR cycle using mathematical modeling. In that study, the heat extracted from the hot water exiting the humidifier was reused by the system. In addition, the VAR condenser was used as the heat source for the HDH system. The results showed that GOR could be improved by increasing the temperature and mass flow rate. Chen et al. [11] compared the efficiency of simple and hybrid HDH systems. They indicated that the HDH setup with an evaporative cooling system boasts higher efficiency at different temperatures and mass flow rates, considering the assumed target mass flow rate (25 – 125 L/h) and GOR (1.6 – 2.5). Faegh and Shafii [12] proposed a hybrid HDH–VCR system in which the heat exiting the VCR condenser was used to evaporate water in the humidifier. The humid air would then be passed through the VCR operator to produce fresh water. They presented that with an increase in the VCR operator temperature (2-14°C), the water production rate and the GOR experienced a notable augment. Many researchers have also studied these systems [13, 14].

In recent years, water sources to desalinate are also facing scarcity [15]; hence, these resources must be used efficiently to obtain the highest amount of fresh water. Boligán Rojas assessed and compared several varity of mechanical design for Solar Desalination Processes [16]. The HDH desalination systems consist of a humidifier and a dehumidifier as the main components. These components can use heat from many heat sources. The HDH systems work on the same principle as the natural water cycle, being a small-scale rain setup. There are three HDH cycle configurations; Closed-Air Open-Water (CAOW), Open-Air Open-Water (OAOW), and Open-Air Closed-Water (OACW). HDH systems are either Water-Heated (WH) or Air-Heated (AH) [8]. There have been many studies concerning the improvement of each of these components. A study by Mistry and Mitsos [17] concludes that the OAOW-WH cycles always experience better performance than CAOW-WH cycles, regardless of the relative ambient humidity. In addition to that, CAOW-AH cycles are always more efficient than OAOW-AH cycles, except for the case where the relative ambient humidity is close to 100% [17]. It can be perceived that OA cycles have better performance in humid regions. Sharqawy et al. [18] reported that WH and AH HDH systems offer an approximately equal GOR, while AH cycles need a larger humidifier and smaller dehumidifier in comparison to WH cycles. Zubair et al [19] compared CW and OW systems and concluded that CW systems have a better performance with less cost.

Most of the HDH systems are designed as OW. The cold saline water is generally used as the cooling fluid in the dehumidifier [9, 20]. In CW HDH systems, the water residing in the humidifier experiences increased temperature. This could lead to the condenser temperature rising beyond the dew point, reducing the rate of condensation. This is why most HDH systems are designed as OA so that the hot water in the humidifier can be removed from the cycle. On the other hand, CW HDH systems can desalinate a higher portion of the saline water, thus reducing heat loss due to the removal of the heated water. Thus, CW HDH systems can play a considerable role in the fresh water supply in regions with less access to even saline water and energy. In order to counter this limitation of CW systems, refrigeration cycle operators can be used to cool the humidifier. This also avoids the use of saline water as a coolant, which counters sedimentation in the pipes of the condenser and ultimately reduces the maintenance cost.

In studies regarding hybrid HDH–Refrigeration cycles, there have not been many systems operating by the use of solar energy. As most of these cycles were compressive refrigeration cycles, their input energy would generally be electric, and the heat generation in the refrigeration cycle was used to heat the air/water in the HDH cycle. In addition to that, as the heat generated in the condensers of the refrigeration cycle is easily accessible, the use of solar energy would be neglected. Hence, designing systems that rely mostly on solar energy as the heat source would be of importance. Regarding this matter, replacing compressive refrigeration with absorption refrigeration would be of use. This is due to the fact that absorption cycles use heat directly, and hence, can use solar energy directly. In this method, solar energy can fuel both the refrigeration needed in the dehumidifier unit, as well as the heat in the humidifier unit. In addition, as the input energy is thermal, on days with undesirable weather condition, an electric heater can be used to supply the energy to the cycles. To sum up, the hybrid HDH– absorption refrigeration cycle, can be used to produce fresh water throughout the year. In this study, a hybrid HDH–absorption desalination system will be proposed and the performance will be assessed. The proposed setup will be an OACW cycle, using solar energy as a renewable and clean energy source. In this model, we have proposed the use of an absorption refrigeration cycle in the dehumidifier unit. Finally, the performance of the system will be assessed and fresh

water production rate, COP of the absorption cycle, GOR rate, and economical considerations will be studied.

EXPERIMENTAL STUDY

Description of experimental setup

The proposed model is a hybrid solar HDH – Absorption refrigeration cycle desalination setup. In order to assess the performance of such system, a model setup has been built. The model consists of three main components; a humidification unit, a dehumidification unit, and a solar air heater. The air first enters the heater and is heated by direct sunlight (Figure 1). In order to control the temperature throughout the process, an electric heater is also used as an equivalent to solar energy. This also helps to assess the performance of the system in different weather conditions. The heated air is then directed towards the humidification unit through an insulated vent. The air enters the humidifier from the bottom and saline water is sprayed from the top. The humid air then exits the humidifier through the top region and is directed towards the dehumidifier. The mass flow rate of the air is controlled by a fan. The residual saline water from the humidifier is recollected and resprayed to humidify the heated air that enters to the humidifier. The water level in the reservoir is controlled by an automatic valve that opens when the level drops and maintains a fixed water level.

In the next stage, the humidified air enters the dehumidification unit through another insulated vent. The dehumidification unit is an absorption refrigeration cycle, in which heat is absorbed from the humidified air. In this stage, the air is brought into direct contact with an ammonia absorption chiller operator and is cooled beneath the dew point temperature, in which condensation occurs and produces fresh water. In order to increase the rate of heat transfer in the dehumidification process, aluminum fins are placed on the surface of the chiller. The dehumidified air is then returned to the ambient. The system is shown in Figure 2 and the relevant information can be found in Table 1.

Measuring equipment

All relevant parameters are measured in order to assess the performance of the setup. These parameters include dry-bulb temperature, prior to and after entering the humidifier and dehumidifier, water temperature prior to and after entering the humidification unit, as well as the absorption refrigeration evaporator surface temperature. In addition to the parameters already mentioned, the mass flow rates of the air and water are also defined.

Type k thermocouples are used to measure the temperature in all experiments. The thermocouples are connected to an ATMEGA32 microcontroller. In order to
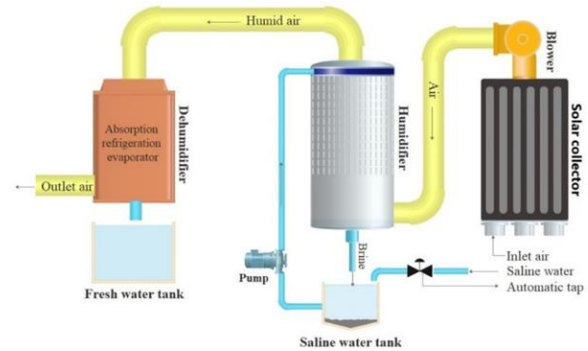

Figure 1. Schematic diagram of the proposed HDH desalination system

Figure 2. Fabricated experimental setup

Table 1. System components and their specifications [21]

| Component	Specifications
Humidifier	Rectangular cross-section, 850×650 mm^2 area with 2000 mm height, made of galvanized iron, insulated with polystyrene on the inside and glass-fiber on the outside
Absorption chiller	83 Watts heat input from the generator and 100 Watts maximum refrigeration power output
Dehumidifier	U-shaped tube with a diameter and length of 22 and 500 mm, respectively. Coated with aluminum heat sinks (Figure 3) which are in turn fully coated by glass wood insulation
Solar air-heater	Rectangular cube with dimensions of 2000×1000 mm^2 by 200 mm width made of galvanized iron sheet with a glass cover on it
Electric heater	Maximum power output of 3500 Watts and 0.07 kg/s flow rate
Saline water reservoir	Cylindrical reservoir made of plastic, supporting a total volume of 10 liters
Air vent	Made of galvanized iron sheets with a circular cross-section with a diameter of 100 mm, insulated by glass wood
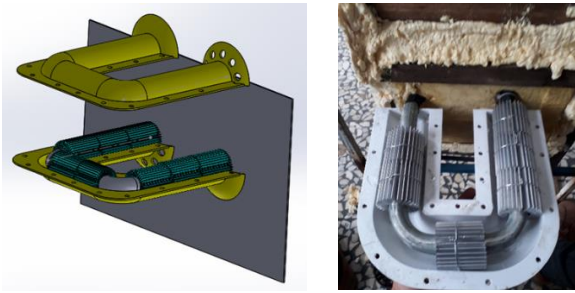
Figure 3. Absorption chiller evaporator (Dehumidifier unit)

measure the water flow rate, a sample reservoir is filled with the water and the required time is measured through a stopwatch. Air velocity is also measured via an anemometer. The accuracy of the measurement setup is presented in Table 2.

Uncertainty analysis
Considering the large number of experimental data, the uncertainty analysis was assessed for the temperature and velocity of the air, leaving the humidifier. For this experiment, the temperature of the inflow air was fixed at 40 °C with a mass flow rate of 0.0025 kg/s. Equations (1) through (4) were used for this analysis [22], and the results are presented in Table 3.

$$\bar{x} = \frac{\sum_{i=1}^{n} x_i}{n} \tag{1}$$

$$s = \sqrt{\frac{\sum_{i=1}^{n}(x_i - \bar{x})^2}{(n-1)}} \tag{2}$$

$$u = \frac{s}{\sqrt{n}} \tag{3}$$

$$U = ku_c \tag{4}$$

where $\bar{x}$ is the mean value, x is the analysis parameter, n is the number of experiments, s is the standard deviation,

Table 2. Measuring equipments used in this study [23]

Instrument	Measurement accuracy	Image
Velocity meter (GM816A)	0.1 (m/s)	
Temperature and humidity sensor (AM1001)	0.1(°C) for Temperature 3% for humidity	

u is the uncertainty and U is the combined uncertainty with a coverage factor of k. According to the data presented in Table 3, the reliability of the experimental data stands at over 95% [24].

Experiment design
As explained earlier, the HDH desalination setup is aimed to be fueled by solar energy. However, in order to control the temperature in different weather conditions, an electric heater is used instead of the solar air heater. In order to find appropriate settings for the heater to match solar radiation, a series of tests were conducted on the solar setup, in the northern region of Iran (Mazandaran Province, Babol city) during the summer. Multiple parameters including the temperature of the surrounding, the mass flow rate of water entering the humidifier, power input to the refrigeration cycle, and power usage of the pump were recorded during the experiments (Table 4). The power input to the electric heater (relevant to solar radiations as explained earlier) and the air mass flow rate were considered as the variables that affect the final performance of the setup. The parameters were measured by fixing the mass flow rate of air into the humidifier (for 0.0025 kg/s air mass flow rate) and the input power to the electric heater and measuring the parameters in the steady-state. Each flowrate was experimented with 4 different system temperatures (40, 50, 60, and 70 °C) to find the best performance of the system.

Performance parameters
Multiple parameters were analyzed in order to assess the performance of this desalination setup. These parameters include fresh water production, input water mass flow rate, GOR, COP, η_H, and η_{DH}. Following the extraction of experimental data, the thermodynamic equations for conservation of mass and energy were employed and studied for each component of the system, to assess the overall performance of the setup. It is noteworthy that the mass flow rate of air ($\dot{m}_a$) is assumed to be constant throughout the process. The equations are presented below.

The value of thermal power input to the air by the solar heater is calculated using Equation (5).

$$\dot{Q}_{collector} = \dot{m}_a C_p (T_{i,h} - T_\infty) \tag{5}$$

The governing equations for the performance of the humidifier are as presented below:

$$\dot{m}_{sw,i,h} = \dot{m}_{sw,o,h} + (\dot{m}_a(\omega_{o,h} - \omega_{i,h}) \tag{6}$$

$$\dot{m}_{a_{i,h}} = \dot{m}_{a_{o,h}} = \dot{m}_a \tag{7}$$

$$\dot{Q}_{loss,h} = \dot{m}_a C_p (T_{o,h} - T_{i,h}) + \dot{m}_{sw,o,h} h_{sw,o,h} - \dot{m}_{sw,i,h} h_{sw,i,h} + \dot{m}_a \omega_{o,h} h_{v,o,h} \tag{8}$$

Table 3. Proposed system uncertainty analysis

Parameter	1	2	3	4	5	Average	Standard deviation	Average uncertainty	Modifed uncertainty
Dehumidifer outlet temprature	22.4	22.4	22.3	22.5	22.3	22.4	0.0836	0.037	0.074
Velocity of humidifier outlet air flow	3.1	3.0	2.9	3.0	2.9	3.0	0.0212	0.009	0.018

Table 4. Constant quantities at different experiments

Quantity	Unit	Value
Ambient temperature	°C	30
Electric heater power of chiller	W	86
Pump power	W	65
Blower power	W	36
Humidifier inlet brine mass flow rate	$Kg/_s$	0.014

The efficiency of the humidifier (η_H) is calculated using Equation (9).

$$\eta_H = \frac{(\omega_{o,h} - \omega_{i,h})}{(\omega_{o,h,s} - \omega_{i,h})} \tag{9}$$

The absolute humidity ($\omega_{o,h,s}$) is when the air exiting the humidifier is fully saturated.

The governing equations for the performance of the dehumidifier are presented below.

$$\dot{m}_{fwp} = \dot{m}_a(\omega_{i,dh} - \omega_{o,dh}) \tag{10}$$

$$\dot{m}_{a_{i,dh}} = \dot{m}_{a_{o,dh}} = \dot{m}_a \tag{11}$$

$$\dot{Q}_e = (\dot{m}_{fwp} \times h_{fg}) + \dot{m}_a(h_{o,dh} - h_{i,dh}) \tag{12}$$

The efficiency of the dehumidifier (η_{DH}) is calculated using Equation (13).

$$\eta_{DH} = \frac{(\omega_{i,dh} - \omega_{o,dh})}{(\omega_{i,dh} - \omega_{o,dh,s})} \tag{13}$$

The absolute humidity ($\omega_{o,h,s}$) is when the air exiting the dehumidifier is fully saturated, while at the temperature of the surface of the dehumidifier.

The dimensionless parameter GOR, denoting the ratio of the latent heat for condensation to the total thermal power input to the system, is calculated using Equation (14).

$$GOR = \frac{h_{fg} \times \dot{m}_{fwp}}{\dot{Q}_{collector} + \dot{Q}_g} \tag{14}$$

The specific latent heat of distillation(h_{fg}) and the thermal power input to the absorption chiller generator ($\dot{Q}_g$) are assumed to be constant and equal to 83 Watts.

The Coefficient of Performance (COP) is the ratio of cooling by the chiller to the input heat to the generator and was only studied for the dehumidifier in this setup (Equation 15) [25].

$$COP = \frac{\dot{Q}_e}{\dot{Q}_g} \tag{15}$$

RESULTS AND DISCUSSION

In order to assess the performance of the desalination setup, the effects of the temperature and air mass flow rate entering the humidifier were considered as the main variables of this experimental study. Parameters such as usefulness, saline water mass flowrate, the efficiency of each component, GOR, and COP were analyzed to assess the performance of the setup. The economic analysis for the desalination setup were also studied. It is noteworthy that the experiments were performed in Iran in July 2021.

Fresh water production
The production of fresh water in constant air mass flow rate at different $T_{a,i,h}$ was studied. As evident from Figure 4, the production of fresh water increases with an increase in temperature, for all mass flow rates. This can be justified by the fact that $T_{a,i,d}$ increases with an increase in $T_{a,i,h}$. This causes the air to accommodate more humidity, and more moisture enters the dehumidifier section per kilogram of dry air. In addition to that, evaporation occurs at a faster rate at higher temperatures. Another parameter affected by an increase in temperature is the dew point temperature. As air temperature increases, the dew point temperature increases, and this, in turn, leads to an increase in the rate of condensation.

The effects of input air to the chiller on the overall COP were studied in another experiment. The experiment showed that COP increases by increasing the input air temperature (Figure 13). This increase in the COP leads to an increase in the cooling power, as the input power to the chiller is constant. This increase in the cooling power leads to augmentation in the rate of water production. The rate of water production in the constant air flow rate of 0.0025 kg/s is approximately a linear function of temperature; however, with an increase in air flow rate, this linear dependency turns into a parabolic relation. According to Figure 5, desalination rate is linearly related to air mass flow rate at constant $T_{a,i,h}$. With an increase in $T_{a,i,h}$, the slope of the line increases. This is due to the fact that a higher flow rate would mean that a larger amount of vapor enters into the dehumidifier per unit time. In addition to that, $T_{a,i,d}$ increases with augmentation in $T_{a,i,h}$, which causes the dew point temperature to go beyond the
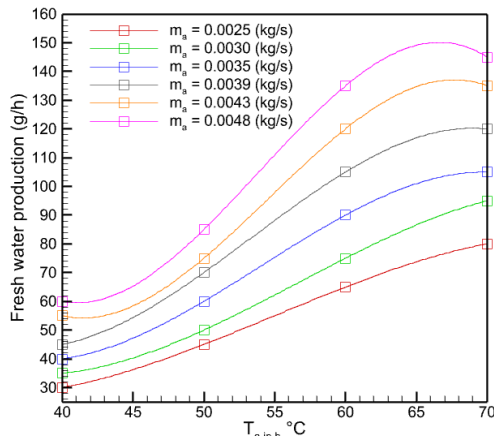
Figure 4. Humidifier inlet air temperature effect on produced fresh water at different air mass flow rates
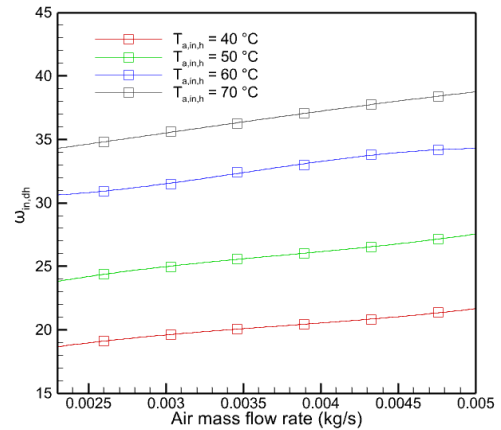

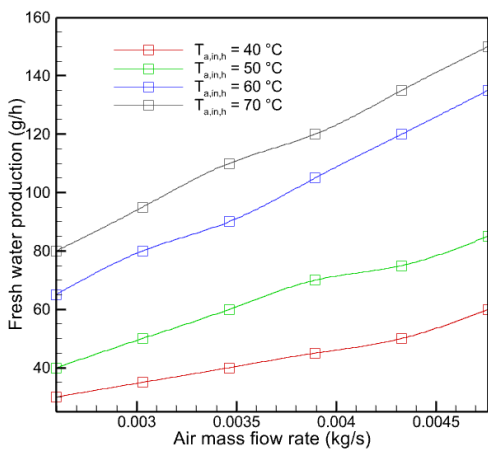**Figure 6.** Air mass flow rate effect on humidifier outlet absolute humidity at different temperatures

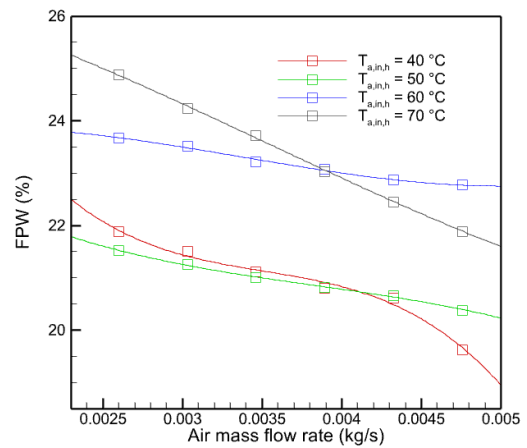**Figure 5.** Air mass flow rate effect on produced fresh water at different temperatures

Figure 7. The effect of air mass flow rate on FPW at different temperatures

surface temperature of the operator. This in turn leads to a greater slope in the rate of water production – air flowrate graph. Another factor contributing to augment in the slope of the water production – air flowrate graph, is an increase in COP at higher temperatures, which was explained earlier.

Saline water entering the system
Considering the fact that the proposed system accommodates a CW cycle, the level of saline water in the reservoir drops over time. In order to counter this, saline water is regularly added to the reservoir. According to Figure 6, the absolute humidity at the outlet of the humidifier increases with an increasing the air mass flow rate. The same can be said about increasing the air temperature. As the absolute humidity can be considered as a scale for the amount of water evaporation, the system would need more saline water at higher air mass flow rates and temperatures. The effect of air mass flow rate on FPW at different temperatures is shown in Figure 7. The
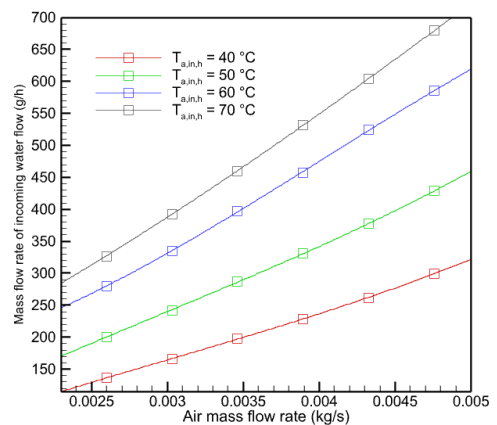

Figure 8. The effect of air mass flow rate on humidifier inlet brine water

amount of saline water consumption by the system was found to be between 136 and 680 g/h (Figure 8). Another parameter that was studied during the experiments, was

the FWPIW. The FWPIW is the ratio of the produced fresh water to the input saline water. As can be perceived from Figure 6, the FWPIW is inversely proportional to the air mass flow rate and directly proportional to temperature. It was found that the optimal FWPIW can be achieved for a flow rate of 0.0025 kg/s and temperature of 70 °C, converting 25% of the saline water to fresh water. The rest of the saline water would leave the control-volume as humidity and leakage.

Humidifier efficiency

The efficiency of the humidifier ranges between 91 to 93%, increasing with increased $T_{a,i,h}$; However, the rate of augmentation decreases. This is mainly due to the fact that higher temperature enables the humidity carriage of a larger amount. In addition to that, isobaric augmentation in temperature, increases the rate of surface evaporation, enabling the air to be humidified, nearly to the fully saturated condition. According to the psychrometric chart, the absolute humidity at the outlet of the humidifier increases at higher temperatures; which increases the efficiency, as shown in Equation (9). The decaying rate of augmentation can be justified by the fact that the air accommodates less humidity, as it approaches the fully-saturated condition; hence, the rate of efficiency augmentation decreases. The effect of humidifier inlet air mass flow rate changes on its efficiency at different air mass flow rates is shown in Figure 9.

As can be seen in Figure 10, the efficiency increases with an augment in the inlet air mass flow rate. The increasing trend is greater in lower temperatures. As the efficiency of the humidifier does not experience a significant change in temperatures 60 and 70 °C, it can be included that at high temperatures, the efficiency of the humidifier is independent of the air flow rate. This is due to the fact that the inlet air enthalpy increases as a result of an increase in the mass flow rate. Assuming that other independent parameters remain unchanged, it is expected that the rate of evaporation increases with an augment in the inlet enthalpy. Furthermore, a higher air flow rate enables higher collision of air molecules with water particles, increasing the rate of evaporation. As a result of these phenomena, the air can be humidified to the point of being fully saturated. The effect of humidifier inlet air temperature on its efficiency at different air mass flow rates is shown in Figure 11. Also the effect of air mass flow rate on humidifier efficiency at different temperatures is shown in Figure 12.

Dehumidifier efficiency

The dehumidifier efficiency is a parabolic function of temperature at high air mass flow rates. It shows an increasing trend with an increase in temperature. Although the parabolic relation becomes linear at lower air mass flow rates, the efficiency still increases with
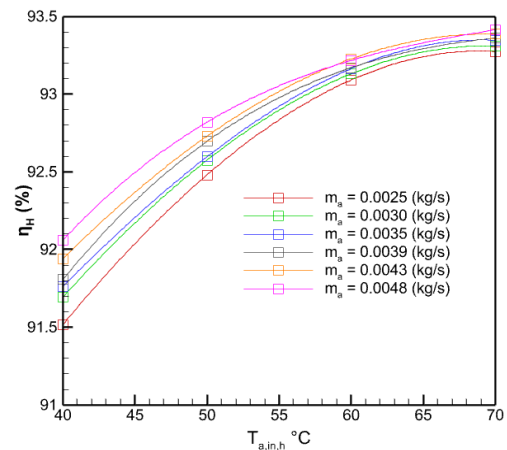

Figure 9. The effect of humidifier inlet air mass flow rate changes on its efficiency at different air mass flow rates
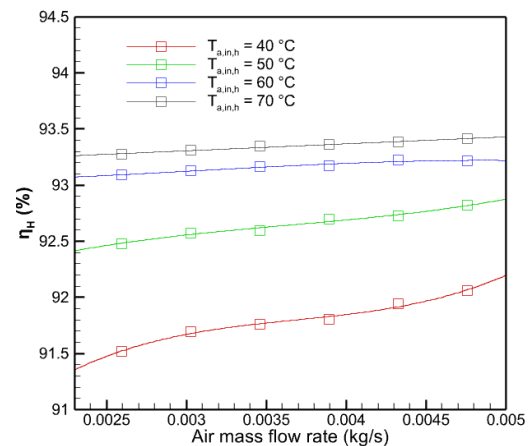

Figure 10. The effect of air mass flow rate changes on humidifier efficiency at different temperatures

temperature. In order to justify this behavior, the performance of the dehumidifier was assessed in another experiment. In the mentioned experiment, dry air entered the dehumidifier at temperature T_i and exits at temperature T_o. As evident in Figure 13, COP is directly proportional to the inlet air temperature and increases from 0.37 to 0.84 as the temperature increases. The highest COP was obtained in the case at 74 °C. As the signifies increased cooling in the humidifier. An increase in the humidifier inflow air temperature, causes an augment in the dehumidifier inflow air temperature.

Higher inlet air flow temperature leads to a higher rate of heat transfer from the chiller operator, which in turn leads to a higher rate of condensation. According to Figure 12, an increased air mass flow rate results in the decay of dehumidifier efficiency. This can be justified by the fact that a higher air mass flow rate signifies higher velocity, limiting the time for heat transfer. This reduces the rate of condensation and with an increase in absolute
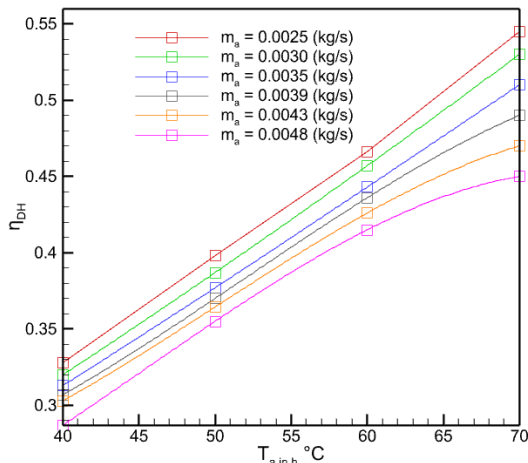
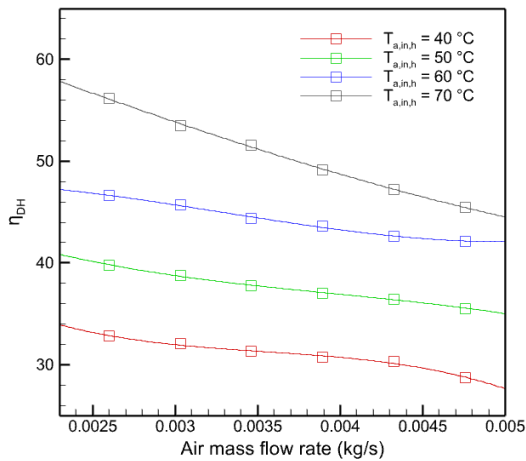**Figure 11.** The effect of humidifier inlet air temperature on its efficiency at different air mass flow rates

Figure 12. The effect of air mass flow rate on humidifier efficiency at different temperatures
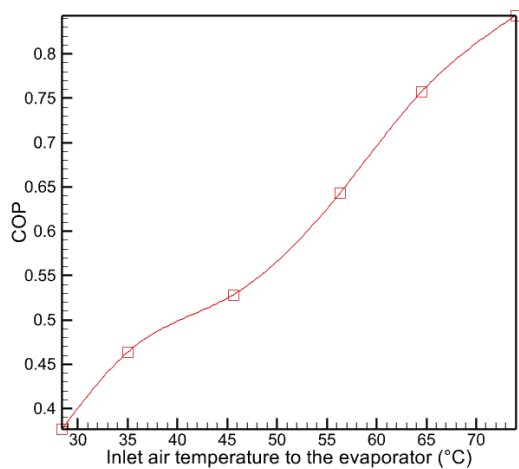

Figure 13. The effect of evaporator inlet air temperature on absorption chiller COP

humidity at the exit of the dehumidification unit, the efficiency of the dehumidifier is reduced. To sum it up, the most efficient condition for the performance of the dehumidifier is the air mass flow rate of 0.0025 kg/s and temperature of 70 °C, which resulted in 56% efficiency.

GOR

Increment in the air mass out flow rate from the heater causes increased thermal input to the desalination cycle. GOR is directly proportional to the amount of fresh water produced and inversely proportional to the total thermal input to the system. Increased thermal input would have a negative impact on the GOR, while increased fresh production would lead to a positive impact on the GOR. Figure 14 displays the superimposed effectiveness of these two parameters. As it is evident, GOR behaves as a third-degree function of temperature; decaying as temperature increases. The GOR remains nearly constant at temperatures 50 and 60 °C, but experiences a rapid drop at 70 °C, dropping to 0.54. This is while GOR increases to a significant value of 1.2 at 40 °C. Considering the fact that the experiments were conducted in the northern region of Iran where the air is considerably humid, heating the inflow air does not have a significant impact on the humidity.

In order to maintain a constant temperature difference between the air inlet and the air outlet of the heater, a higher air mass flow rate would require more thermal energy. In case of a solar heater, the air mass flow rate can be adjusted to be higher during the hours that the sun radiation is more intense. In this condition, an increased air mass flow rate would also result in increased thermal energy input to the system, culminating in an increased rate of fresh water production. Equation (14) shows that GOR is directly proportional to fresh water mass flow rate and inversely proportional to the thermal energy input. As can be perceived from Figure 15, GOR remains nearly constant at higher temperatures and is not a function of air mass flow rate; however, when the air temperature reaches 40 °C, the GOR initially increases with air mass flow rate, reaching a peak at the air mass flow rate 0.0045 kg/s, and decays with an increase in air mass flow rate.

Economic analysis

The economic analysis and fresh water cost estimation of the proposed desalination system plays a crucial role in the effectiveness of the setup. The overall fixed cost of this model (F) was estimated to be approximately $137.5 (Table 5 and 6). The lifetime of the HDH setup (n) was assumed to be 10 years, and the annual earning rate was assumed to be 10%. The Capital recovery factor (CRF) and the sinking fund factor (SFF) are defined below:

$$CRF = i(1 + i)^n/[(1 + i)^n - 1] \tag{16}$$
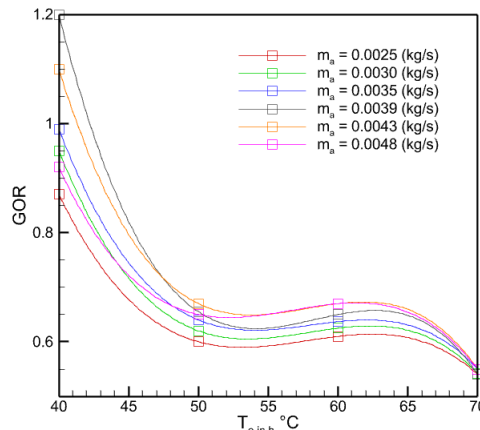
$$SFF = i/[(1 + i)^n - 1] \tag{17}$$

Figure 14. The effect of inlet air temperature to humidifier on GOR in different air mass flow rates
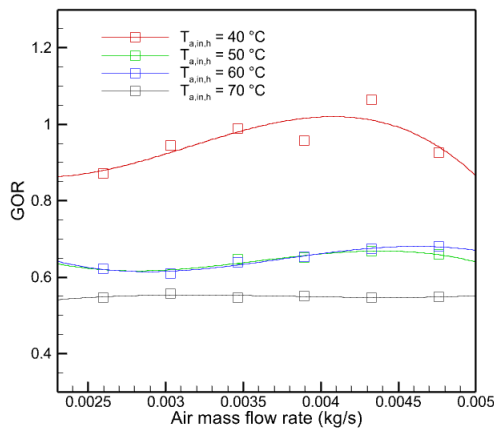

Figure 15. The effect of Air mass flow rate on GOR at different temperatures

The first annual cost (FAC) is obtained by multiplying F by CRF.

$$FAC = F \times CRF \tag{18}$$

Insurance cost (S) was assumed to be 20% of the fixed cost, as presented below:

$$S = 0.2 \times F \tag{19}$$

Annual insurance value (ASV) is obtained by the multiplication of S by SFF, as presented below.

$$ASV = S \times SFF \tag{20}$$

Annual maintenance cost (AMC) was estimated to be 15% of the first annual cost, as proposed in similar studies [14, 26]. The use of electrical energy was considered as the only parameter contributing to annual recurring costs (ARC) (Equation 26).

$$ARC = 365\tau (P_B + P_P + P_{ACH})C_{ele} \tag{21}$$

Assuming that the system operates for 14 hours a day (τ) and the cost of electricity (C_{elec}) as $0.127 per kilowatt-

hour, ARC can be estimated. Annual cost (AC) can be obtained as below.

$$AC = FAC + AMC + ARC - ASV \tag{22}$$

Table 5. Required initial investment

Parameter	Unit	Value
F	USD	137.5
N	Year	10
I	%	10
CRF	-	0.162
SFF	-	0.062
FAC	USD	22.3
S	USD	27.5
ASV	USD	1.7
AMC	USD	3.3
ARC	USD	102
AC	USD	125.9
AC_{fw}	USD	0.16

Table 6. Estimated cost of the proposed desalination system

Component	Fixed cost ($)
Pump	8
Blower	6
Absorption Chiller	40
Humidifier	35
Fiberglass insulation	3.5
Pipes and fittings	10
Solar air heater	25
Ancillary costs	10
Total (F)	137.5

Table 7. Result comparison of related studies

References	Year	Solar energy used or not	Cooling system used or not	Production	GOR	CFW
Zhang et al. [26]	2019	No	No	29.2	2.57	0.14
Faegh et al. [8]	2020	No	Yes	1.08	2	0.019
Santosh, et al. [20]	2020	No	Yes	4.7	1.27	0.04
Chen, et al. [11]	2020	No	Yes	140	2.4-1.6	–
Mohamed, et al. [27]	2020	Yes	No	6.16	0.86	0.012
Alsehli, et al. [28]	2021	Yes	No	1.8-0.05	1.9-0.03	–

Finally, the cost per kilogram (AC$_{fw}$) can be estimated (assuming 0.15 kg/h fresh water production) as below.

$$AC_{fw} = AC/(365\tau \times m_{fw}) \tag{23}$$

The CPL was calculated to be 0.16 in the present study. As can be seen in Table 7, the value for CPL is relatively higher in the present study. Considering the fact that the size of the setup is smaller than the other studies, the losses are more significant. In addition to that, the cost of fabrication is higher in smaller scales.

CONCLUSION

The present study investigated the performance of an HDH desalination setup coupled with an ammonia absorption refrigeration chiller. One of the notable aspects of the proposed design is that the system operates mainly on solar energy. The electric heater can be used when the weather condition is undesirable. Parameters such as input air flow temperature and air mass flow rate were studied and the economic analysis was also presented at the end. The findings can be concluded as:

- The highest rate of water production and GOR were found to be 150 g/h and 1.2, respectively. Increasing mass flow rate, increases the rate of water production and COP while reducing the efficiency of the dehumidifier. The efficiency of the humidifier, however, remains nearly constant. On the other hand, increasing input air flow temperature, reduces GOR, while other parameters show an increasing trend with temperature.
- The results show that at higher temperatures, the rate of water production increases; hence, water production drops during the hours with less solar radiation. The hybrid heat supply system enables the setup to operate at more efficient temperatures.
- The GOR is more desirable when the temperature is lower. This is due to the fact that the air is rather humid and the system requires less thermal energy to operate the humidification unit. This enables the setup to operate for more hours using solar energy. The relative operation is also more desirable, even during undesirable weather conditions.
- The use of the Ammonia absorption refrigeration cycle along with the HDH desalination setup, enables the conversion of saline water to fresh water with a ratio as high as 25%. Furthermore, thermal waste is also avoided and the dehumidifier boasts up to 93% efficiency.
- Increased mass flow rate causes a decay in the efficiency of the dehumidifier. Contrary to the mass flow rate, increased input water temperature leads to an increase in the efficiency of the dehumidifier. Hence, the efficiency of the dehumidifier decays during hours

of undesirable radiation, which is countered by the employment of the hybrid heating system.
- The economic analysis of the present model indicated a CPL value of $0.16/L; which is higher in comparison to other studies. This can be justified by the smaller dimensions of the device, which causes the losses to be more significant. In addition to that, the hybrid system contains more components to operate, even during nighttime.

REFERENCES

1. Van Vliet, M. T., Jones, E. R., Flörke, M., Franssen, W. H., Hanasaki, N., Wada, Y. and Yearsley, J. R., 2021. Global water scarcity including surface water quality and expansions of clean water technologies, *Environmental Research Letters,* 16(2), pp. 024020. Doi:10.1088/1748-9326/abbfc3

2. Elbassoussi, M. H., Ahmed, M., Zubair, S. M. and Qasem, N. A., 2021. On a thermodynamically-balanced humidification-dehumidification desalination system driven by a vapor-absorption heat pump, *Energy Conversion and Management,* 238, pp. 114142. Doi:10.1016/j.enconman.2021.114142

3. Mohamed, A., Ahmed, M. S. and Shahdy, A. G., 2020. Theoretical and experimental study of a seawater desalination system based on humidification-dehumidification technique, *Renewable Energy,* 152, pp. 823-834. Doi:10.1016/j.renene.2020.01.116

4. Zubair, M. I., Al-Sulaiman, F. A., Antar, M., Al-Dini, S. A. and Ibrahim, N. I., 2017. Performance and cost assessment of solar driven humidification dehumidification desalination system, *Energy Conversion and Management,* 132, pp. 28-39. Doi:10.1016/j.enconman.2016.10.005

5. Orfi, J., Galanis, N. and Laplante, M., 2007. Air humidification–dehumidification for a water desalination system using solar energy, *Desalination,* 203(1-3), pp. 471-481. Doi:10.1016/j.desal.2006.04.022

6. Soomro, S. H., Santosh, R., Bak, C.-U., Kim, W.-S. and Kim, Y.-D., 2021. Humidification-dehumidification desalination system powered by simultaneous air-water solar heater, *Sustainability,* 13(23), pp. 13491. Doi:10.3390/su132313491

7. Cichoń, A. and Worek, W., 2021. Analytical Investigation of a Novel System for Combined Dew Point Cooling and Water Recovery, *Applied Sciences,* 11(4), pp. 1481. Doi:10.3390/app11041481

8. Faegh, M., Behnam, P. and Shafii, M. B., 2019. A review on recent advances in humidification-dehumidification (HDH) desalination systems integrated with refrigeration, power and desalination technologies, *Energy Conversion and Management,* 196, pp. 1002-1036. Doi:10.1016/j.enconman.2019.06.063

9. Lawal, D., Antar, M., Khalifa, A., Zubair, S. and Al-Sulaiman, F., 2018. Humidification-dehumidification desalination system operated by a heat pump, *Energy Conversion and Management,* 161, pp. 128-140. Doi:10.1016/j.enconman.2018.01.067

10. Lawal, D. U., Zubair, S. M. and Antar, M. A., 2018. Exergo-economic analysis of humidification-dehumidification (HDH) desalination systems driven by heat pump (HP), *Desalination,* 443, pp. 11-25. Doi:10.1016/j.desal.2018.05.011

11. Chen, Q., Burhan, M., Shahzad, M. W., Ybyraiymkul, D., Akhtar, F. H. and Ng, K. C., 2020. Simultaneous production of cooling and freshwater by an integrated indirect evaporative cooling and humidification-dehumidification desalination cycle, *Energy Conversion and Management,* 221, pp. 113169. Doi:10.1016/j.enconman.2020.113169

12. Faegh, M. and Shafii, M. B., 2020. Thermal performance assessment of an evaporative condenser-based combined heat pump and humidification-dehumidification desalination system, *Desalination,* 496, pp. 114733. Doi:10.1016/j.desal.2020.114733

13. Dehghani, S., Date, A. and Akbarzadeh, A., 2018. Performance analysis of a heat pump driven humidification-dehumidification desalination system, *Desalination,* 445, pp. 95-104. Doi:10.1016/j.desal.2018.07.033

14. Shafii, M. B., Jafargholi, H. and Faegh, M., 2018. Experimental investigation of heat recovery in a humidification-dehumidification desalination system via a heat pump, *Desalination,* 437, pp. 81-88. Doi:10.1016/j.desal.2018.03.004

15. Yassin, M., 2020. Development of Integrated Water Resources Planning Model for Dublin using WEAP21, Doctoral thesis, Technological University Dublin.

16. Boligán Rojas, G., Lorenzo Ávila Rondon, R. and Carolina Meléndez Gurrola, A., 2018. Mechanical Engineering Design Theory Framework for Solar Desalination Processes: A Review and Meta-Analysis, *Iranian (Iranica) Journal of Energy & Environment,* 9(2), pp. 137-145. Doi:10.5829/IJEE.2018.09.02.09

17. Mistry, K. H. and Mitsos, A., 2011. Optimal operating conditions and configurations for humidification–dehumidification desalination cycles, *International Journal of Thermal Sciences,* 50(5), pp. 779-789. Doi:10.1016/j.ijthermalsci.2010.12.013

18. Sharqawy, M. H., Antar, M. A., Zubair, S. M. and Elbashir, A. M., 2014. Optimum thermal design of humidification dehumidification desalination systems, *Desalination,* 349, pp. 10-21. Doi:10.1016/j.desal.2014.06.016

19. Zubair, S. M., Antar, M. A., Elmutasim, S. M. and Lawal, D. U., 2018. Performance evaluation of humidification-dehumidification (HDH) desalination systems with and without heat recovery options: An experimental and theoretical investigation, *Desalination,* 436, pp. 161-175. Doi:10.1016/j.desal.2018.02.018

20. Santosh, R., Kumaresan, G., Kumar, G. K. and Velraj, R., 2020. Experimental parametric investigation of waste heat powered humidification dehumidification system for production of freshwater from wastewater, *Desalination,* 484, pp. 114422. Doi:10.1016/j.desal.2020.114422

21. Rezaei Rad, M., Shafaghat, R., Aghajani Afghan, A. and Alizadeh Kharkeshi, B., 2023. An experimental study to evaluate the performance of an HDH water desalination system with a thermoelectric condenser, *Renewable Energy Research and Applications*. Doi:10.22044/rera.2023.12548.1191

22. Kharkeshi, B. A., Shafaghat, R., Jahanian, O., Alamian, R. and Rezanejad, K., 2022. Experimental study of an oscillating water column converter to optimize nonlinear PTO using genetic algorithm, *Energy,* 260, pp. 124925. Doi:10.1016/J.ENERGY.2022.124925

23. Shafaghat, R., Fallahi, M., Alizadeh Kharkeshi, B. and Yousefifard, M., 2022. Experimental evaluation of the effect of incident wave frequency on the performance of a dual-chamber oscillating water columns considering resonance phenomenon occurrence, *Iranian (Iranica) Journal of Energy & Environment,* 13(2), pp. 98-110. Doi:10.5829/IJEE.2022.13.02.01

24. Alizadeh Kharkeshi, B., Shafaghat, R., Jahanian, O. and Alamian, R., 2021. Experimental evaluation of the effect of dimensionless hydrodynamic coefficients on the performance of a multi-chamber oscillating water column converter in laboratory scale, *Modares Mechanical Engineering,* 21(12), pp. 823-834, [In Persian]. Available at: http://mme.modares.ac.ir/article-15-52993-en.html

25. Chahartaghi, M. and Kharkeshi, B. A., 2018. Performance analysis of a combined cooling, heating and power system with PEM fuel cell as a prime mover, *Applied Thermal Engineering,* 128, pp. 805-817. Doi:10.1016/j.applthermaleng.2017.09.072

26. Zhang, Y., Zhang, H., Zheng, W., You, S. and Wang, Y., 2019. Optimal operating conditions of a hybrid humidification-dehumidification and heat pump desalination system with multi-objective particle swarm algorithm, *Desalination,* 468, pp. 114076. Doi:10.1016/j.desal.2019.114076

27. Mohamed, A., Shahdy, A. G. and Ahmed, M. S., 2021. Investigation on solar humidification dehumidification water desalination system using a closed-air cycle, *Applied Thermal Engineering,* 188, pp. 116621. Doi:10.1016/j.applthermaleng.2021.116621

28. Alsehli, M., 2021. A New Approach to Solar Desalination Using a Humidification–Dehumidification Process for Remote Areas, *Processes,* 9(7), pp. 1120. Doi:10.3390/pr9071120

Persian Abstract

چکیده

در این مقاله، عملکرد یک آب‌شیرین‌کن هیبریدی HDH به‌صورت تجربی مورد مطالعه قرار گرفته است. این سامانه به صورت چرخه‌ی آب‌بسته - هواباز (OACW) بوده، از هواگرمکن خورشیدی برای افزایش دمای هوای ورودی به رطوبت‌زا و از اثر خنک‌کنندگی یک سیستم تبرید جذبی برای رطوبت‌زدایی هوای مرطوب و تولید آب شیرین بهره می‌برد. با استفاده از سنسور دما و رطوبت، مقادیر دما و رطوبت نسبی در بخش‌های مختلف چرخه، اندازه‌گیری و ثبت و با استفاده از نرم‌افزار EES سایر خواص ترمودینامیکی در بخش‌های مختلف چرخه محاسبه شده است. در بخش نتایج، تأثیر پارامترهای مختلفی مانند دبی جرمی و دمای هوای ورودی به رطوبت‌زا بر تولید آب شیرین، COP، GOR و راندمان رطوبت‌زا و رطوبت‌زدا بررسی شده است. تجزیه و تحلیل نتایج تجربی نشان داد که بیشترین تولید آب و GOR به ترتیب به ۱۵۰ و ۱/۲ g/h می‌رسد. همچنین، مشاهده شد که افزایش دبی هوا منجر به افزایش تولید آب و COP می‌شود؛ ولی مقادیر GOR و راندمان رطوبت‌زدا کاهش می‌یابد. این در حالی که است راندمان رطوبت‌زا تقریباً ثابت می‌ماند. علاوه بر این مشاهده شد که افزایش دمای هوای ورودی به رطوبت‌زا منجر به کاهش GOR می‌شود ولی سایر پارامترها با افزایش دما روندی صعودی دارند. با توجه به تجزیه و تحلیل اقتصادی، CPL در مطالعه حاضر ۰/۱۶ دلار بر لیتر بدست آمد.